

Matrix stiffness modulates tip cell formation through the p-PXN-Rac1-YAP signaling axis

Yaru Guo^a, Feng Mei^{b,c}, Ying Huang^a, Siqin Ma^a, Yan Wei^a, Xuehui Zhang^{d,e,f}, Mingming Xu^a, Ying He^a, Boon Chin Heng^g, Lili Chen^{b,c,*}, Xuliang Deng^{a,d,e,f,**}

^a Department of Geriatric Dentistry, Peking University School and Hospital of Stomatology, Beijing, 100081, China

^b Department of Stomatology, Union Hospital, Tongji Medical College, Huazhong University of Science and Technology, Wuhan, 430022, China

^c Hubei Province Key Laboratory of Oral and Maxillofacial Development and Regeneration, Wuhan, 430022, China

^d Department of Dental Materials, Peking University School and Hospital of Stomatology, Beijing, 100081, PR China

^e National Engineering Laboratory for Digital and Material Technology of Stomatology, Beijing, 100081, PR China

^f Beijing Laboratory of Biomedical Materials, Peking University School and Hospital of Stomatology, Beijing, 100081, PR China

^g Central Laboratory, Peking University School and Hospital of Stomatology, Beijing, 100081, PR China

ARTICLE INFO

Keywords:

Tip cells
Mechanotransduction
Stiffness
Angiogenesis
Extracellular matrix

ABSTRACT

Endothelial tip cell outgrowth of blood-vessel sprouts marks the initiation of angiogenesis which is critical in physiological and pathophysiological procedures. However, how mechanical characteristics of extracellular matrix (ECM) modulates tip cell formation has been largely neglected. In this study, we found enhanced CD31 expression in the stiffening outer layer of hepatocellular carcinoma than in surrounding soft tissues. Stiffened matrix promoted sprouting from endothelial cell (EC) spheroids and upregulated expressions of tip cell-enriched genes *in vitro*. Moreover, tip cells showed increased cellular stiffness, more actin cytoskeleton organization and enhanced YAP nuclear transfer than stalk and phalanx ECs. We further uncovered that substrate stiffness regulates FAK and Paxillin phosphorylation in focal adhesion of ECs promoting Rac1 transition from inactive to active state. YAP is subsequently activated and translocated into nucleus, leading to increased tip cell specification. p-Paxillin can also loosen the intercellular connection which also facilitates tip cell specification. Collectively our present study shows that matrix stiffness modulates tip cell formation through p-PXN-Rac1-YAP signaling axis, shedding light on the role of mechanotransduction in tip cell formation. This is of special significance in biomaterial design and treatment of some pathological situations.

1. Introduction

Angiogenesis, in which new blood vessels are generated via endothelial cell (EC) sprouting from preexisting vessels, is critical to the survival and efficacy of tissue regeneration [1,2]. Once angiogenesis is initiated, the sprouting process is spearheaded by specialized ECs termed tip cells [3–5]. The specification of tip cells is a key point in angiogenesis and tissue engineering because of its directional migration into the avascular area and decisive role in the morphology of blood vessels finally formed [6–8]. To date, various factors, such as such as MST1–FOXO1 [3], VEGF [9,10], DLL4–Notch1 [2], microRNA-30

(miR-30) [11], activin receptor-like kinase 1 (ALK1) [12], SRY-related HMG box 17 (SOX17) [13] and transcription factor NF-E2-related factor 2 (Nrf2) [7] have been reported to be tip cell regulators, and the underlying mechanisms in which these modulate tip cell formation have been extensively studied. However, these are all biochemical signaling molecules, whereas the establishment of functional vasculature requires a combination of both biochemical and biomechanical signaling cues. The latter is dependent on the properties of biomaterials utilized in tissue engineering and regenerative medicine, which provide three-dimensional (3D) extracellular-matrix (ECM) environments [14]. Therefore, exploring the role of ECM mechanical cues in regulating tip

Peer review under responsibility of KeAi Communications Co., Ltd.

* Corresponding author. Department of Stomatology, Union Hospital, Tongji Medical College, Huazhong University of Science and Technology, Wuhan, 430022, China.

** Corresponding author. Department of Geriatric Dentistry, Peking University School and Hospital of Stomatology, Beijing, 100081, China.

E-mail addresses: chenlili1030@hust.edu.cn (L. Chen), kqdengxuliang@bjmu.edu.cn (X. Deng).

<https://doi.org/10.1016/j.bioactmat.2021.05.033>

Received 19 March 2021; Received in revised form 5 May 2021; Accepted 19 May 2021

Available online 1 June 2021

2452-199X/© 2021 The Authors. Publishing services by Elsevier B.V. on behalf of KeAi Communications Co. Ltd. This is an open access article under the CC

BY-NC-ND license (<http://creativecommons.org/licenses/by-nc-nd/4.0/>).

cell specification might help optimize biomaterials to enhance angiogenesis.

Vasculature has long been recognized as being naturally mechano-sensitive to various biomechanical stimuli, including shear stress and pulsatile luminal pressure, which are associated with modulation of vascular phenotypes [15,16]. ECs express many mechanosensors, including G-protein-coupled receptors [17], and ion channels [18] within the luminal layer to sense shear stress, PECAM-1 [19], VE-Cadherin [20] within the junctional layer and integrins within the basal layer to sense ECM properties [16]. With the development of biomaterials, ECM mechanical cues have been shown to participate in proliferation, survival, spread and motility of ECs through mechanotransduction mediated by integrins and the following phosphorylated FAK and paxillin (PXN) [15,21–24]. ECM stiffens in many pathological processes, including cancer and wound healing [25,26], which remarkably promotes angiogenic outgrowth and branching of ECs [27]. Moreover, rigid ECM can activate YAP in a Hippo/LATS-cascade-independent manner [28]. As a universal mechanotransducer and mechanoeffector, YAP has been recently described to regulate tip cell specification [29–31]. Therefore, it is tempting to speculate that ECM stiffness can modulate tip cell specification and angiogenic initiation through YAP-mediated-mechanotransduction. Accordingly, this study aims to explore if mechanotransduction imposed by ECM stiffening promotes tip cell formation through YAP activation as well as the upstream regulatory mechanisms that orchestrate the mechanosensitive integrin and YAP.

In this study, we have examined the effects of matrix stiffness on tip cell formation and explored the underlying mechanisms. We found higher CD31 expression in the outer layer of hepatocellular carcinoma (HCC) with higher tissue stiffness than in surrounding tissue of lower tissue stiffness. Matrix stiffening led to significantly more vessel outgrowth, sprouting and increased expression of tip cell-enriched genes *in vitro*. Mechanistically, stiff matrix increased FAK and paxillin phosphorylation (p-PXN) in focal adhesion. Then p-PXN elevated the level of active Rac1, which resulted in increased cytoskeleton organization and cellular stiffness. Subsequently, YAP, as downstream mechanoeffector, was activated and translocated into nucleus, upregulating the expression of the target genes and eventually promoting tip cell formation. Moreover, p-PXN could also decrease intercellular connection, thus enhance tip cell formation. Together, our present work not only help seek for the optimal materials in tissue engineering and regenerative medicine but also provide novel treatment strategy for oncotherapy and pathological angiogenesis.

2. Materials and methods

2.1. Fluorescent immunohistochemistry

Tissue processing and sectioning were performed as previously described [32]. Briefly, tissue samples were fixed for 2 days with 10% (w/v) neutral formalin and dehydrated according to standard protocols. Next, after embedded in paraffin, 5 mm thick sections of samples were prepared. Then, the sections were deparaffinized and rehydrated, followed by antigen retrieval in a microwave oven (800 W for 20 min). The slides were subsequently washed with PBS three times for 5 min each. The sections were blocked with 5% (w/v) BSA in PBS for 30 min, and then incubated with the primary antibodies anti-CD31 (ab28364, Abcam) overnight at 4 °C. Then, the sections were washed three times with PBS and incubated with the secondary antibodies, Alexa Fluor-594 (ab150080; Abcam), for 1 h at room temperature. The nuclei were stained by DAPI. The sections were washed by PBS for three times before fixation using Fluoromount-G (00-4958-02; Thermo Fisher scientific, Rockford, IL, USA). Eventually, the coverslips were finally sealed using nail polish. Pictures were captured under confocal microscopy.

2.2. Animals and surgical procedures

The animal surgical procedure was approved by the Institutional Animal Care and Use Committee of Peking University (Number: LA2019297). 20 male Balb/c nude mice (8 weeks old) with cells injected with 5×10^6 HepG2 cells subcutaneously were purchased from the Beijing HFK Bioscience Co. Ltd. (Beijing, China). After 8 days, for exploring the effect of matrix stiffness on angiogenesis, experimental group (n = 5) were intraperitoneally injected with 100 μ l 100 mg/kg beta-aminopropionitrile (BAPN) [33], and the control rats with the saline. For exploring the effect of YAP inhibitor on angiogenesis, the YAP inhibitor verteporfin (VP, 25 mg/kg) was given to the YAP inhibitor group (n = 5) [34]. After four weeks, implants were harvested.

For retinal vessel formation *in vivo*, C57BL/6 N mouse pups at P4 were used. 0.5 μ g Rac siRNA was injected intravitreally into one eye and control siRNA was injected into the other eye [35]. Retinas were harvested 2 days later. Flat mounted, fixed tissues were stained with FITC-conjugated isolectin B4 and imaged using a confocal laser scanning microscopy. Then tip cell number was quantified using Image J.

2.3. Patients and tissue samples

This project was approved by the Peking University Third Hospital Medical Science Research Ethics Committee (Number: IRB00006765-M2019543). All clinical samples were obtained from patients (n = 5) with HCC who had undergone surgical excision at the Peking University Third Hospital (Beijing, China). Informed consent was obtained from all patients in accordance with institutional guidelines.

2.4. Generation of endothelial cell spheroids

Agarose (2% w/v) was used to form a mould for endothelial cell (EC) spheroids, whilst preventing adhesion of cells to the mould surface. The agarose (2% w/v) was heated to form a melted solution and then added into a 3D Petri Dish (Microtissues®). After solidification, the agarose moulds were placed in a six-well plate for culturing cells. Then, 180 μ l of cell suspension was seeded on each mould. Twenty minutes later, the culture medium was added and cellular aggregates were allowed to form for 24 h.

2.5. The spheroid-based sprouting angiogenesis model

For the *in vitro* sprouting angiogenesis assay, spheroids were generated overnight, after which they were embedded into gelatin methacryloyl (GelMA) gels (EFL, China). After light curing, culture medium was added. The spheroids were allowed to sprout for a few hours. Then, *in vitro* sprouting was quantitated digitally by measuring the number of extensions and the length of the sprouts (calculated as cellular invasion distance) that had grown out of each spheroid using the Image Pro Plus software, and analyzing 8–10 spheroids per experimental group.

2.6. Mechanical test of GelMA gels

GM-30/60/90 solution was prepared with deionized water, in which the photoinitiator was 0.25% (w/v). 200 μ l was injected into a die with a diameter of 8 mm. After light curing by 405 nm light source for 90s, the cylindrical sample was put on the hydrogel micro-force tester (EFL-MT-5600, EFL) and the stress-strain curve was drawn. The first 10% slope of the strain on the stress-strain curve was taken as its compression modulus.

2.7. Mechanical test of subcutaneous tumors

Stiffness detection of subcutaneous tumors was performed based on previous studies with modification [27,36]. Briefly, the freshly isolated subcutaneous tumor samples were flash-frozen and were thawed in PBS

only immediately before mechanical testing was performed. Tumor stiffness was measured with a universal testing machine (Instron, USA). Specifically, after rehydration in PBS for 20 min, cylindrical biopsies (4 mm diameter, 4 mm thick) were excised from the tissue samples by a biopsy punch. Then, the biopsies were subjected to compressive loads at 1 mm/min crosshead speed until fracture, and the elastic modulus was computed from the stress-strain curve.

2.8. RT-qPCR analysis

Using a PCR thermal cycler (Takara), reverse transcription was achieved. Then the optical adhesive films (Thermo Fisher Scientific) and optical 96-well reaction plates (Thermo Fisher Scientific) were used for PCR. Then, data were analyzed using QuantStudio Design & Analysis Desktop Software (Thermo Fisher Scientific). The primer sequences are shown in Table S1. GAPDH served as the internal control.

2.9. Cell culture

Human primary cell lines, human umbilical vein endothelial cells (hUVECs), were purchased from ScienCell Research Laboratories and cultured in endothelial cell medium (ECM, 1001; ScienCell Research Laboratories), within a humidified chamber at 37 °C with 5% CO₂.

2.10. Lentiviral vector production and transfection

The lentivirus respectively encoding Cdh5, GFP-paxillin (PXN) gene and the PXN phosphorylation mutants, in which both tyrosine 31 and 118 were replaced by phenylalanine (non-phosphorylatable), was purchased from GeneChem Co., Ltd. (Shanghai, China).

One day before transfection of lentiviruses, hUVECs were seeded in six-well plates at 40% confluence. Next, lentiviruses were added to the cell culture with 5 mg/mL polybrene (GeneChem) for 12 h. Subsequently, transfected cells were selected using puromycin (P8833; Sigma-Aldrich) for 3 days.

2.11. Western blot

Western blot was performed as previously described [32]. The following antibodies were used: anti-GAPDH (ab9485; Abcam), anti-paxillin (610568, BD), anti-FAK (610087, BD), anti-p-FAK (Tyr397) (44-624G, ThermoFisher), anti-p-paxillin (Tyr118) (44-722G, ThermoFisher), anti-p-paxillin (44-720G, ThermoFisher), anti-Rac1 (507720, Zenbio), anti-VE-Cadherin (ab33168; Abcam), anti-integrin α 5 (ab6131; Abcam), anti-integrin β 1 (ab183666; Abcam), anti-integrin β 3 (ab197662; Abcam), anti-vinculin (ab129002; Abcam). The secondary antibody was HRP-labeled IgG (A0208, A0216; Beyotime).

2.12. Atomic force microscopy (AFM)

AFM force spectroscopy experiments were performed with the operation mode of PeakForce QNM in Fluid available on a commercial AFM BioScope Re-solve (Bruker, Billerica, MA, USA). Force mappings were obtained using a silicon nitride probe (PFQNM-LC-A-CAL, Bruker) with pre-calibrated spring constant of 0.091 N/m, tip height of 17 μ m, and tip radius of 65 nm. Deflection sensitivity of the cantilever was calculated by thermal tune. Force curves were captured by Force Volume mode with scan size of 500 nm, ramps/line of 4, ramp rate of 1 Hz, ramp size of 1.5 μ m and deflection error trigger threshold of 6 nm. All force curves were treated with Sneddon model in Nanoscope Analysis software (Bruker) to extrapolate the apparent Young's modulus with tip half angle of 18° and sample poisson's ratio of 0.5. All experiments were done at room temperature in ECM within 1 h. Above 16 force mappings were obtained per sample, and 30 different samples were analyzed for each condition.

2.13. Detachment protocols of cells in FluidFM BOT

Adhesion force of cell to substrate with different stiffness was measured with FluidFM BOT according to previous study [37]. All measurements regarding to cell adhesion forces were performed by FluidFM BOT system (Cytosurge AG, Switzerland) which combines AFM and microfluidics technology. Tipless FluidFM BOT micropipette probe (Cytosurge AG, Switzerland) with microfluidic channels was used with a 4 μ m aperture at distal and a nominal spring constant of 0.3 N/m. About 1 μ l of filtered ddH₂O was loaded into the liquid reservoir of hollow cantilever using a hand held pipette. Then the probe was immersed in 0.1 mg/mL of PACrAm-g-(PMOXA, NH₂, Si) (SuSoS AG, Switzerland) solution to coat its exterior for 30 min to prevent fouling and washed in filtered ddH₂O for 5 min subsequently. The spring constant (k) and deflection sensitivity of the cantilever was calibrated by a Cytosurge software built-in procedure before cell adhesion measurements. The system was mounted on an IX83 inverted microscope (Olympus, Japan) to target the individual cells for detachment. Cells were approached at 3 μ m/s with a setpoint of 100 nN. When the probe was attached to the cells reaching the setpoint, pressure of -650 mbar was applied in the cantilever reservoir holding for 5s to ensure sealing the cell to the cantilever. Then the probe retracted to a height of 100 μ m maintaining the pressure of -650 mbar with the speed of 1 μ m/s to detach the cells from the substrate completely. Both Z stage height and force-distance curve were recorded per cell and analyzed for adhesion strength. At least 20 force-distance curves were captured for each condition. All cell adhesion measurements were recorded at 37 °C in a humidified 5% CO₂ incubation chamber.

2.14. Immunofluorescence analysis

The samples were rinsed with PBS and then fixed with 4% paraformaldehyde for 10 min at room temperature. Subsequently, the samples were permeabilized with 0.1% Triton X-100 for 10 min and blocked with 5% bovine serum albumin (BSA; diluted with PBS) for 1 h at room temperature. The samples were incubated with the following primary antibodies in 5% BSA in PBS overnight at 4 °C: anti-paxillin (610568, BD), anti-FAK (610087, BD), anti-p-FAK (Tyr397) (44-624G, ThermoFisher), anti-p-paxillin (Tyr118) (44-722G, ThermoFisher), anti-Rac1 (507720, Zenbio), anti-NO-1 (13663S, Cell Signaling Technology) and anti-YAP1 (14074S, Cell Signaling Technology). After removing excess antibody and rinsed with PBS for 3 times, the samples were incubated with the following secondary antibodies for 1 h in the dark: donkey anti-rabbit IgG H&L Alexa Fluor 594 (ab150080, Abcam) and Goat anti-mouse IgG H&L Alexa Fluor 647 (ab150115, Abcam) goat anti-rabbit IgG H&L Alexa Fluor 488 (ab150077, Abcam). Phalloidin (Sigma) was used for cytoskeletal staining. Nuclei were stained using 4',6-diamidino-2-phenylindole (DAPI; Sigma). Images were captured using a confocal laser scanning microscope (Leica).

For quantifications of YAP subcellular localizations, YAP immunofluorescence signal was scored as predominantly nuclear (the nuclear/cytoplasmic ratios > 1.25) versus evenly distributed (the nuclear/cytoplasmic ratios are 0.75–1.25)/predominantly cytoplasmic (the nuclear/cytoplasmic ratios < 0.75) in 40 cells according to previous study [38]. The percentage of cells with predominantly nuclear YAP was used to quantify YAP activation.

2.15. Rac1-GTP pulldown assays

Rac1-GTP pulldown assay was performed using the thermo scientific active rac1 pull-down and detection Kit. Briefly, cells were lysed in ice-cold lysis buffer supplemented with protease inhibitors. Cleared lysates were incubated with GST-human Pak1-PBD for 30 min at 4 °C under end-to-end rotation. The beads were washed, boiled in Laemmli buffer, and Western blotted. The Western blot bands were quantified using the software program ImageJ. Bar graphs represent RhoA GTP/input RhoA.

GTP-Rac1 were pulled down using GST-PAK1-PBD beads.

2.16. Inhibitor selection

Y-27632 (10 μ M) [34], NSC23766 (50 μ M) [39], EHT1864 (20 μ M) [40], Src inhibitor 1 (Srci, 2 μ M), FAK inhibitor defactinib hydrochloride (FAKi, 1 μ M and 3 μ M for low and high concentration [41], respectively) and Verteporfin (VP, 5 μ M and 10 μ M for low and high concentration, respectively) [42] were all purchased from Medchemexpress, New Jersey, America.

2.17. Statistical analysis

Results were expressed as mean \pm SEM. Analysis between more than two sample groups was performed by a one-way unstacked ANOVA and post-hoc LSD testing. Analysis between two paired samples was

performed by a two-tailed unpaired Student's *t*-test. P values less than 0.05 were considered statistically significant.

3. Results and discussion

3.1. Extracellular matrix stiffness regulates tip cell formation and angiogenesis

Clinically, solid tumors such as HCC is often accompanied by hepatocirrhosis with higher tissue stiffness than surrounding tissue [27]. We found that enhanced CD31 intensity in the outer layer of HCC than surrounding tissues (Fig. S1A), indicating the promotion of angiogenesis in stiffer cancerous tissue. To further explore the relationship between matrix stiffness and angiogenesis, HCC model was created through injecting HepG2 cells subcutaneously into Balb/c nude mice.

BAPN, an inhibitor of the matrix cross-linking enzyme lysyl oxidase

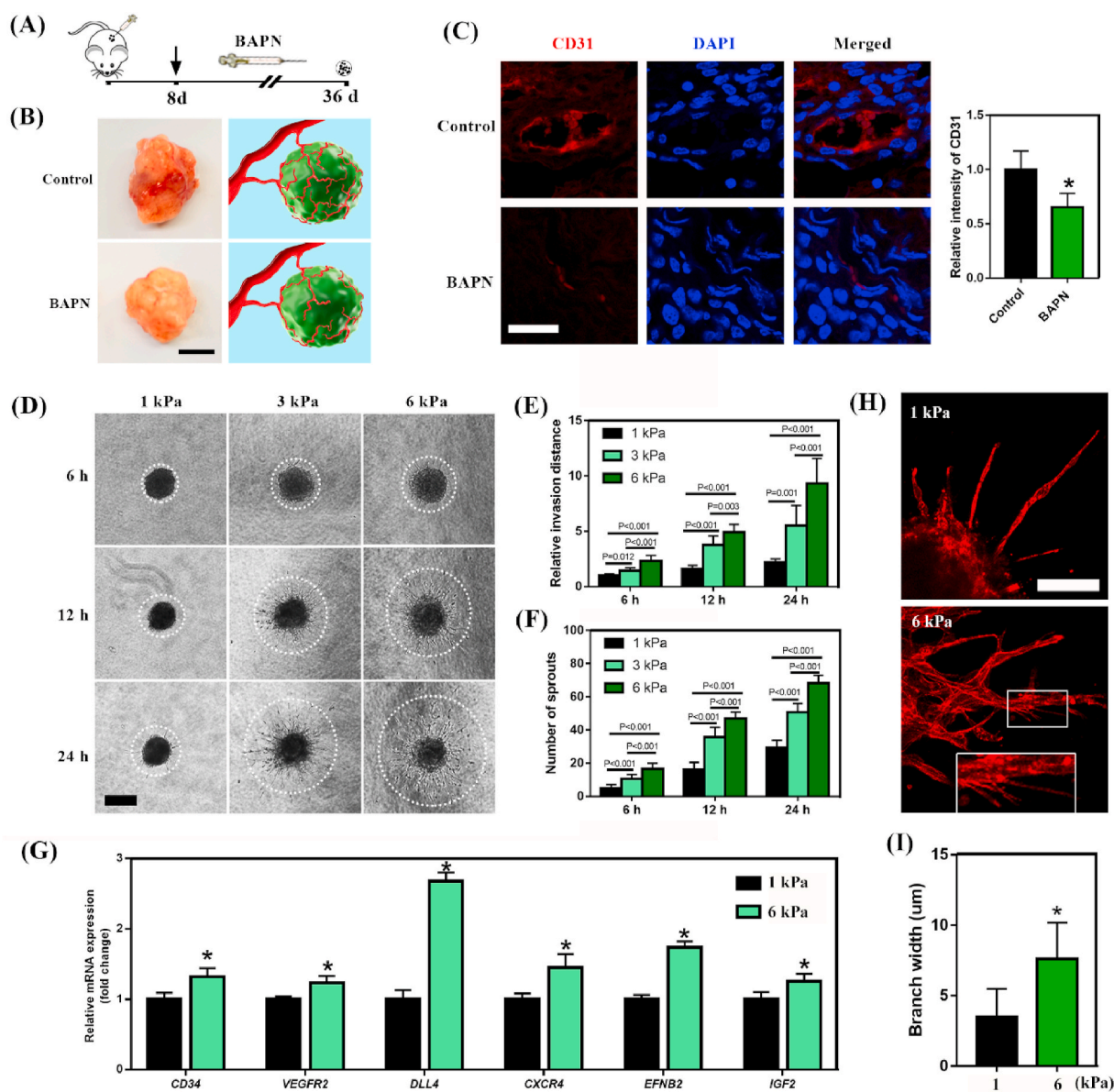


Fig. 1. Matrix stiffening enhances angiogenesis and tip cell formation *in vitro* and *in vivo*. (A) Scheme illustration of BAPN application in nude mice with xenograft. (B) Photographs of implants showed that sprouting angiogenesis of xenograft was significantly reduced by BAPN treatment (Scale bar: 5 mm). (C) Immunocytochemistry showed decreased intensity of CD31 after BAPN treatment. (Scale bar: 25 μ m) (D) Spheroid sprouting assay showed that matrix stiffening promotes the invasive capacity and sprout number of hUVECs, (Scale bar: 200 μ m) and the quantitative analysis is shown in (E) and (F). (G) qPCR showed that the expression of tip cell enriched genes are significantly increased in the stiff matrix. (H) Immunocytochemistry showed thicker extensions with filopodia on stiffer gels (Scale bar: 50 μ m) and the quantitative analysis is shown in (I). (* $p < 0.05$).

(LOX) involved in tumor stiffening, were used once a day for four weeks from the 8th day (Fig. 1A). After one month, we found apparently decreased tissue stiffness in the BAPN treatment group (Fig. 1SB), with dramatically decreased blood vessel branches in tumor capsular angiogenesis (Fig. 1B) and significantly reduced CD31, CD34, VEGF intensity (Fig. 1C and Fig. S2). These results are consistent with previous finding that BAPN injection reduced the mechanical properties and

angiogenesis of the ECM in tumors [43,44]. Therefore, it could be postulated there was closed correlation between ECM stiffness and tip cell formation and angiogenesis.

To further confirm the relationship of ECM stiffness and tip cell formation, we fabricated a biomaterials model in which matrix stiffness can be modulated. Gelatin methacrylate (GelMA) hydrogels were used at the same concentration with different methacrylation degree (GM30,

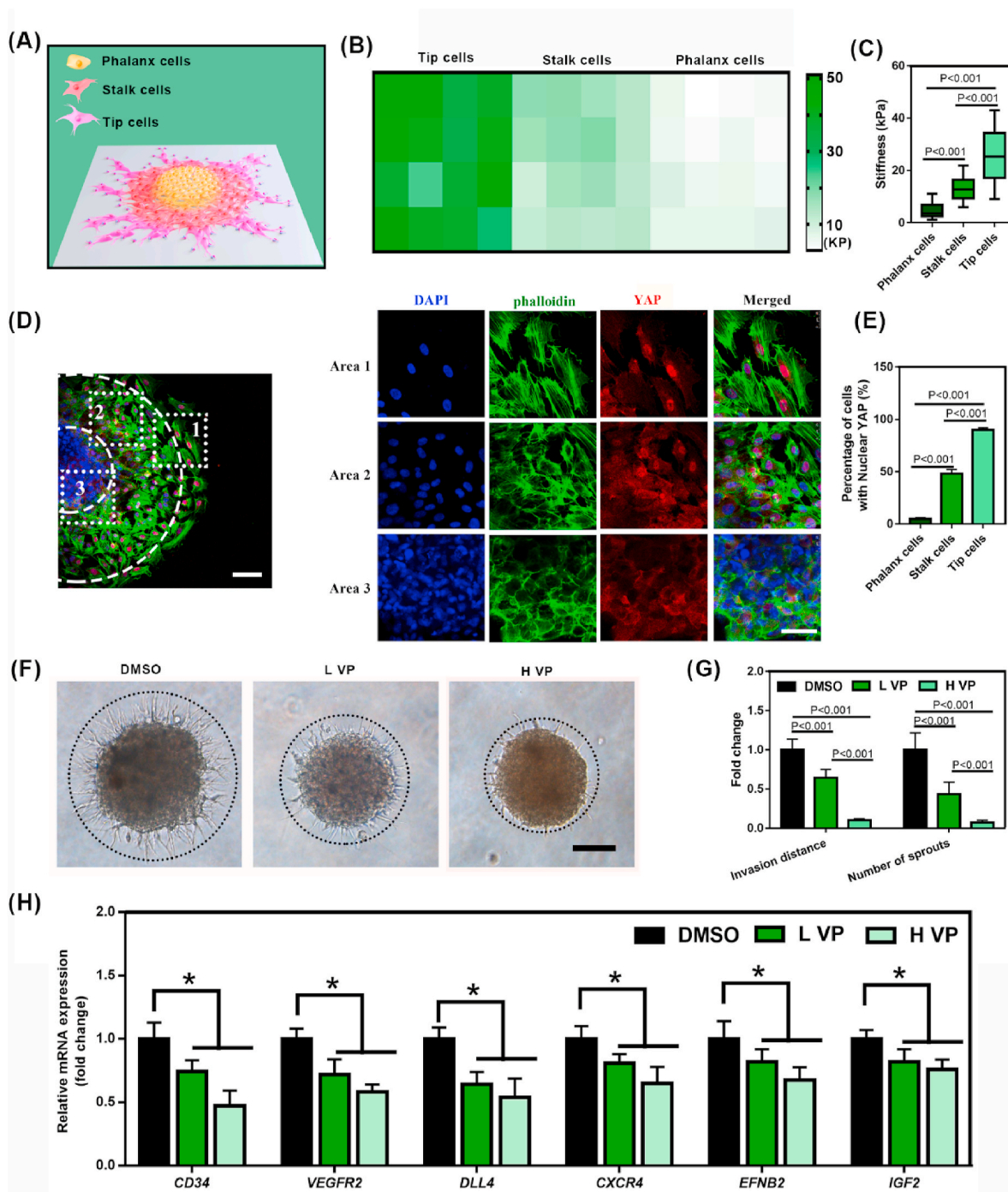


Fig. 2. Mechanical property differences of tip, stalk and phalanx cells. (A) Schematic illustration of tip cells, stalk cells and phalanx cells in hUVEC spheroid spreading. (B) The typical mechanics heatmaps of 16 detected positions of each cell type by AFM. (C) Quantification of stiffness indicated that tip cells were stiffest, followed by stalk cells, while phalanx cells were softest. (D) Immunocytochemical staining showed that tip cells displayed enhanced assembly of long stress fibers (white arrows) and had the most YAP nuclear localization, followed by stalk cells, whereas there was barely any stress fiber and nuclear YAP translocation in the phalanx cells. (Scale bar: 100 μm) (E) Quantification analysis of YAP activation in different cell types. (F) Spheroid sprouting angiogenesis assay showed that VP inhibited sprouting angiogenesis in a concentration-dependent manner. (Scale bar: 100 μm) (G) Quantification analysis of relative invasion distance and sprout numbers in (F). (H) qPCR showed that tip cell enriched genes were decreased significantly by high concentration of VP. (* $p < 0.05$).

GM60, GM90) [45]. As shown in Fig. S3, hydrogel stiffness is increased by increased methacrylation degree and gelatin concentration, from 1 kPa to 70 kPa. Since microelasticity of most soft tissues, including brain, breast, liver, lung and kidney, is less than 6 kPa [46], the effects of GelMA stiffness from 1 kPa to 6 kPa on EC sprouting were investigated. We found that increase in stiffness promoted sprouting angiogenesis (Fig. 1D), as demonstrated by increased invasion distance of sprouts from three dimensional (3D) EC spheroids (Fig. 1E). Since tip cells are responsible for sprouting of angiogenesis, the counted angiogenic sprouts of EC spheroids were often employed as an indicator of tip cell formation [47]. We found that sprouts from spheroids in stiffer gels (GM90) had a 2-fold increase in sprout number compared with those within more compliant gels (GM60 and GM30) (Fig. 1F). qPCR analysis showed that tip cell enriched genes, including *CD34*, *VEGFR2*, *DLL4*, *CXCR4*, *EFNB2* and *IGF2* [48–50], are upregulated significantly in GM90 matrix (Fig. 1G). Meanwhile, the width of sprouts in stiffer gels is thicker with more and long filopodia into the matrix (Fig. 1H and I). Taken together, these data shows that matrix stiffening promotes angiogenesis and tip cell formation.

When the stiffness was increased to 15 kPa by increasing concentration of GelMA gels, we found both sprout number and invasion distance were decreased (Fig. S4). Similar observation of reduced sprouting upon increasing the density of the matrix has been reported in other studies [27,51]. This might be due to that the increase in concentration decreases the porosity of matrix and makes it more difficult for ECs to degrade, deform and remodel, thereby reducing sprouting angiogenesis [51,52]. Tissue stiffness, including HCC, increases with disease progression under pathological circumstances. For example, stiffness of HCC and liver cirrhosis tissues can increase up to about 60 kPa [53,54]. Therefore, to better mimic the stiffness of HCC and eliminate the effects of 3D ECM concentration, we examined two-dimensional (2D) spread of spheroids on substrate with stiffness of between 3 and 70 kPa. The results showed that the spreading distance and sprout number were elevated by increased stiffness (Fig. S5). These different findings between 3D and 2D circumstances suggest that the effects of stiffness on EC sprouting are dependent on the mechanism of stiffening, i.e., increase in stiffness independent of ECM concentration (through cross-linking of enzymes) or through increased ECM density [55].

3.2. Mechanical properties of tip, stalk and phalanx cell ECs

As matrix stiffness regulates tip cell specification, we therefore characterized the mechanical property of tip cells, stalk cells and phalanx cells (also called static cells). In the EC spheroid sprouting model, the outermost cells and the following cells emerging from spheroids were respectively defined as tip cells and stalk cells. Cells that not clambered out of the spheroid were defined as phalanx cells (Fig. 2A). By atomic force microscopy (AFM), we detected 16 positions of each cells and fabricated the typical mechanics heatmaps (Fig. 2B). Remarkable differences were found among these three kinds of cells. The stiffness of tip cells was quantitatively twice that of stalk cells and four times that of phalanx cells (Fig. 2C). Moreover, immunofluorescence staining showed that tip cells displayed enhanced assembly of long stress fibers while in stalk and phalanx cells actin bundles were relatively short and restricted to the cell periphery (Fig. 2D). Since increased tension of actin cytoskeleton, reflected by cellular stiffness, has been considered linked to YAP activation [28,56], we therefore wonder if three subtypes of ECs are different in subcellular distribution of YAP. We found that YAP in tip cells showed obvious nuclear localization, while YAP became predominantly cytoplasmic in phalanx cells (Fig. 2D and E). Accordingly, differences of cellular stiffness, actin cytoskeletons and subcellular YAP distribution indicated distinct mechanical properties among tip, stalk and phalanx ECs. By immunofluorescence, FluidFM BOT system and AFM, we found increased cell spreading areas (Fig. S6A), adhesive forces (Figs. S6B and C) and cellular stiffness (Fig. S6D) of ECs on rigid substrate, indicating increased EC-ECM connection and promoted cell

mechanical property by ECM stiffening. To verify that YAP was involved in matrix stiffness-induced tip cell specification, verteporfin (VP), a YAP inhibitor, was used in sprouting angiogenesis assay. We found that VP treatment remarkably decreased the extension number and sprout invasion distance of EC spheres in a concentration dependent manner (Fig. 2F and G). The tip cell enriched genes was also declined by VP (Fig. 2H). Therefore, it could be inferred that the matrix stiffening modulates the cellular mechanical perception and mechanotransduction of ECs, promotes YAP activation, which eventually enhances tip cell formation.

3.3. ECM stiffness regulates tip cell formation through PXN phosphorylation

Having established the mechanical differences among EC subtypes in angiogenesis and tip cell formation, we next sought to explore how ECM stiffness are interpreted by ECs and how downstream mechanotransduction events are elicited to modulate cellular mechanobiology and tip cell specification. Adhesion to the ECM is mediated by specialized complex across plasma membrane called focal adhesions (FAs), which are intrinsically mechanosensitive and play a central role in mechanochemical conversion [24]. We thus analyzed the components of focal adhesions (FAs) by western blots. We found that ECs cultured in stiffer matrix showed increased phosphorylation levels of FAK and paxillin (PXN) (Fig. 3A). Immunofluorescence staining also showed higher intensity of p-FAK and p-PXN on stiffer substrate, especially in the lamellipodium area of hUVECs (Fig. 3B and Fig. S7). We then used small molecule inhibitors targeting Src (Srci) and phosphorylation of FAK at 397 (FAKi) to explore the effect of p-FAK and p-PXN on tip cell formation. We found that spheroids treated with FAKi showed a significant reduction in sprouting extension (Fig. S8). Angiogenic sprouts was most completely blocked by FAKi + Srci (Fig. S8).

To further verify the involvement of p-PXN in stiff ECM-induced tip cell specification, we overexpressed PXN in HUVECs with adenovirus transfection. We also constructed a constitutively inactive mutant of YFP-PXN, replacing Y31 and Y118 with phenylalanine (Y2F), rendering the molecule nonphosphorylatable. The transfection was confirmed by Western blot analysis (Fig. 3C). We found that the number and size of FAs were much increased in PXN overexpression group compared with inactive mutant (Fig. S9). AFM showed PXN overexpression dramatically improved the cellular stiffness of hUVECs, while the mutant decreased the stiffness to the vehicle group (Fig. 3D). By qPCR and sprouting angiogenesis experiment, we found that PXN overexpression increased tip cell-enriched genes (Fig. 3E) and facilitated the sprouting from spheroids (Fig. 3F and G), which were inhibited by the mutant. Accordingly, we deduced that PXN phosphorylation is required for tip cell formation imposed by matrix stiffening.

In this study, the stiffness of GelMA hydrogels is elevated by methacrylation degree rather than the concentration of gelatin. The ligand numbers and distribution provided by hydrogels exhibit little variability among different matrix stiffness groups. This might be the reason for small variation detected in other adhesion components, including integrin beta 1, beta 3, vinculin, total FAK and total PXN, when matrix stiffness was increased by modulating the methacrylation degree (Fig. 3A).

FAK and PXN are the mechanosensing proteins in adhesions [41]. They are activated by changing their level of tyrosine phosphorylation in response to increased substrate stiffness, not the number of integrins involved. Therefore, although little variation of vinculin, integrin beta 1 and beta 3 was found in this study, elevated levels of p-FAK and p-PXN indicate more mechanic perception by cells in stiffer matrix and the more mechanical cues converted into biomechanical signaling.

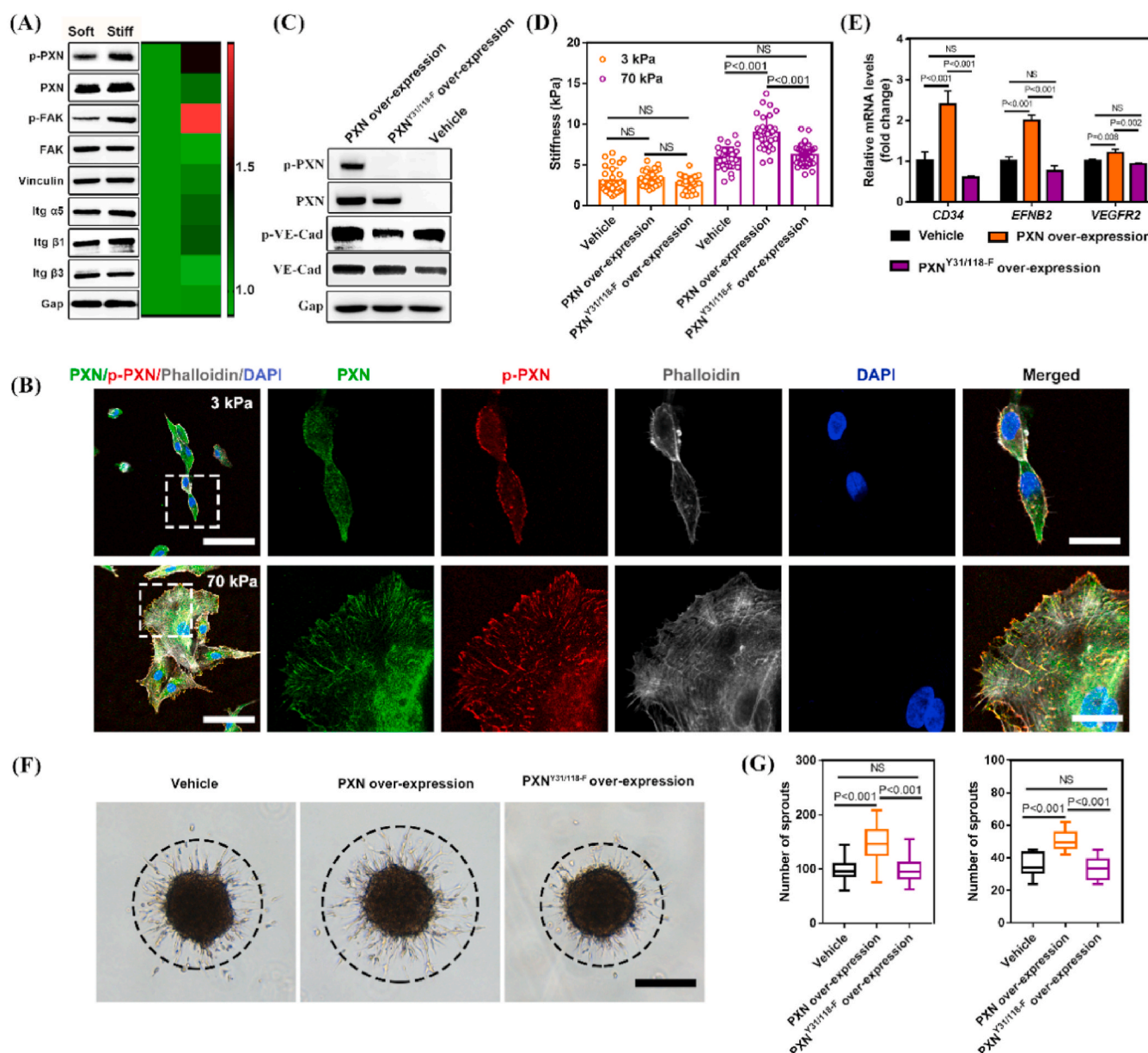


Fig. 3. ECM stiffness regulates tip cell formation through PXN phosphorylation. (A) Western blots showed that ECM stiffening did not affect components of FAs but improved phosphorylation levels of FAK and PXN. (B) Immunocytochemistry showed that matrix stiffening increased p-PXN intensity, particularly at peripheral areas of hUVECs. (Scale bar: left 75 μ m, right 25 μ m) (C) Confirmation of adenovirus transfection. PXN overexpression dramatically enhanced the cellular stiffness (D), expression of tip cell enriched genes (E) and sprouting angiogenesis (F) of hUVECs, which were abolished by the mutant. (Scale bar: 200 μ m) (G) Quantification analysis of relative invasion distance and sprout numbers in (F). (* $p < 0.05$).

3.4. PXN phosphorylation activates Rac-YAP signaling axis in regulation of tip cell formation

We next investigated the intracellular mechanotransduction mechanisms by which PXN phosphorylation enhances tip cell formation. In our research, PCR analysis showed Rac1 and ROCK, the main downstream molecules of RhoA, were higher in stiffer matrix (Fig. S10A). To explore whether Rac1 and ROCK were required for stiffness-induced tip cell formation and angiogenesis, inhibitors of Rac1 (NSC23766 and EHT1864) and ROCK (Y-27632) were used. All of Y-27632, NSC23766 and EHT1864 decreased the branch width of sprouts (Fig. S10B) due to the inhibition on cytoskeleton organization. We found that both NSC23766 and EHT1864, inhibitors of Rac family GTPases, decreased sprouting angiogenesis. On the contrary, Y-27632, inhibitor of ROCK,

led to increased sprout number and invasion length (Fig. S10C). These results indicate Rac1 is responsible for tip cell specification. To explore the Rac1 level in tip cells, stalk cells and phalanx cells, immunofluorescence staining of spreading spheroids was performed. The results showed the highest intensity of Rac1 in tip cell cells, followed by stalk cells, while there was barely Rac activation in phalanx cells (Fig. 4A and B). To determine whether Rac activity is required for tip cell formation under physiological condition, we injected Rac1 siRNA (0.5 μ g) directly into the eyes of 4 days post-natal P4 C57BL/6 N mice (Fig. 4C). After two days, we found that Rac siRNA markedly inhibited developmental retinal angiogenesis, resulting in 20% less tip cells (Fig. 4D and E). Accordingly, all these findings indicate that Rac1 is responsible for angiogenic phenotype and tip cell formation induced by ECM stiffening.

Based on the composition, dynamics and function of molecules,

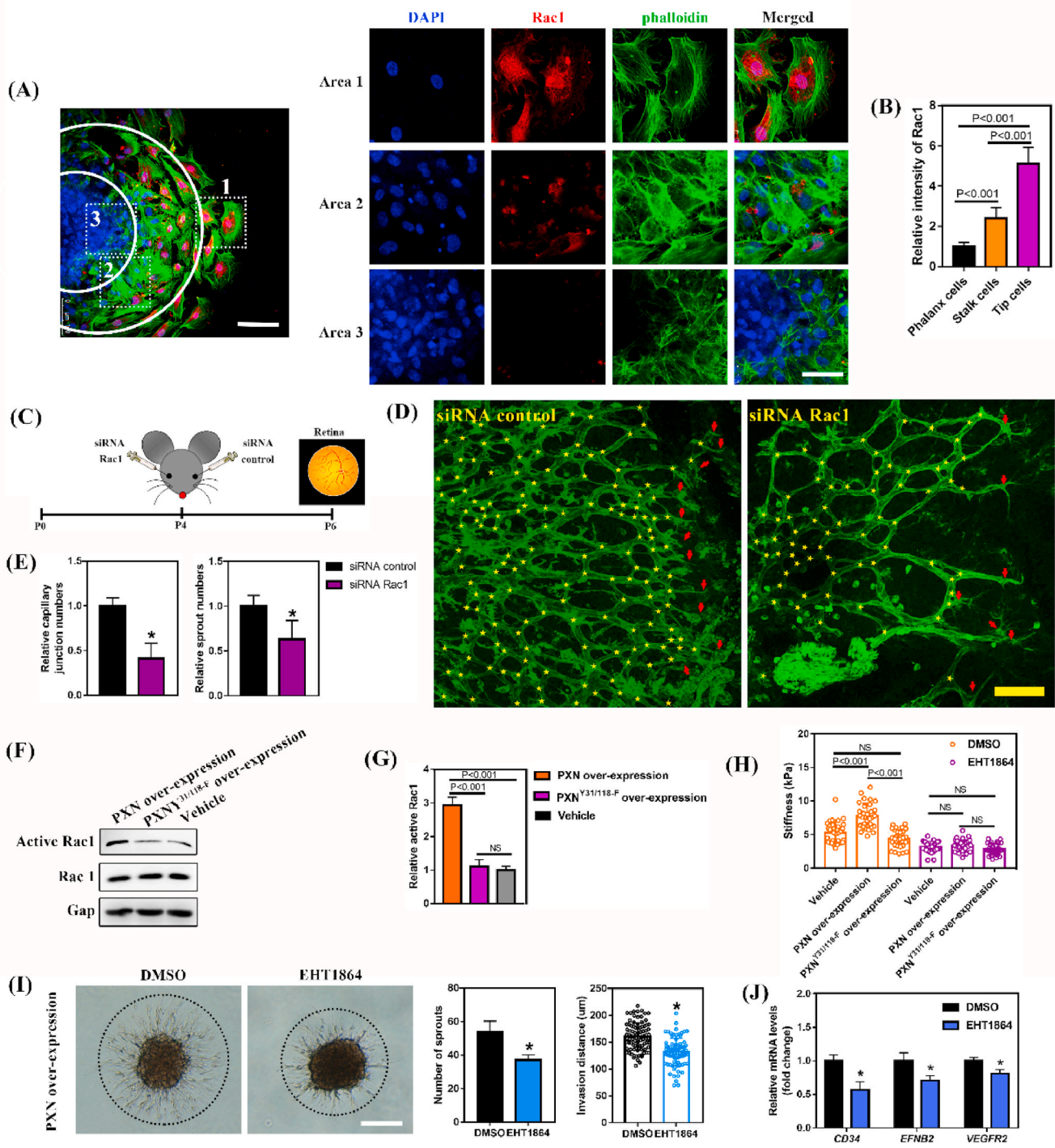


Fig. 4. PXN phosphorylation activates Rac1 to regulate tip cell formation. (A) Immunocytochemical staining showed that tip cells displayed the highest intensity of Rac1, followed by stalk cells, while there was barely any Rac activation in the phalanx cells. (Scale bar: 100 μm) (B) Quantification analysis of Rac1 intensity in different cell types. (C) Schematic illustration of Rac1 siRNA application in retinal angiogenesis. (D) Isolectin B4 staining of the developing retinal vessels treated by siRNA control or siRNA Rac1 at P6 showed that siRNA Rac1 treatment led to impaired retinal development with decreased tip cell number. Red arrows and yellow asterisks marked the angiogenic sprouts and capillary junctions, respectively. (Scale bar: 100 μm) (E) Decreased relative capillary junction numbers and sprout numbers were observed after siRNA Rac1 treatment. (F) Overexpression of PXN increased active Rac1 expression level, which was abrogated by the Y2F-PXN mutant. (G) The quantitative analysis of active Rac1 expression in (F). EHT1864 treatment abrogated PXN overexpression-induced cellular stiffness (H), angiogenic sprouting (I) (Scale bar: 200 μm) and expression of tip cell enriched genes (J). (*p < 0.05).

integrin-induced cell-ECM adhesions can be divided into three types, focal complexes (FXs), focal adhesions (FAs) and fibrillar adhesions (FBs) [57]. FXs are highly dynamic, dot-like adhesions. FXs can mature into FA in a contractility-dependent manner. Then, FAs can transform into more stable FBs under actomyosin contractility [58]. It has been

reported that Rac and Rho participate in regulation of integrin-mediated adhesions [58]. Specifically, Rac activation induces FX development often located in cellular frontier area. While Rho activity often occurs in the formation of FAs and FBs which often exist in cellular center and rear area. This might be the reason why inhibitors of Rac family GTPases

decreased sprouting angiogenesis and inhibitor of ROCK led to increased sprout number and invasion length.

We then explored the relationship between PXN and Rac1 in determining tip cell formation and the final angiogenic phenotype. Like other GTPases, the Rac1 cycles between an active (GTP bound) and an inactive (GDP-bound) state [59]. We wonder whether PXN phosphorylation could lead to more activated Rac1. To this end, we performed a pull-down assay using purified GST-human Pak1-PBD, which specifically binds to Rac1-GTP. We found that compared to the vehicle control, overexpression PXN caused more than three-times increase of the Rac1-GTP amount (Fig. 4F and G). By contrast, mutant PXN showed similar Rac1-GTP with the vehicle group, thereby demonstrating more Rac1 was activated by p-PXN. To further confirm Rac1 as the effector of p-PXN, Rac1 inhibitor EHT1864, which inhibit Rac1-mediated functions directly and rapidly [60], was used. We found that EHT1864 administration abrogated the PXN overexpression-induced cellular stiffness (Fig. 4H), angiogenic sprouting (Fig. 4I) and expression of tip cell-enriched genes (Fig. 4J).

We next explored the effects of p-PXN-Rac1 signaling on the sub-cellular localization of YAP. hUVECs on stiff ECM showed a higher expression and nuclear localization of YAP (Fig. 5A and C) compared with those plated in soft substrate. Then we explored if p-PXN-Rac1 imposed by stiff substrate adjusted the subcellular localization of YAP. We found that PXN overexpression increased YAP nuclear localization. ECs expressing mutant PXN, on the other hand, showed similar percentage of cells with nuclear YAP as the vehicle group. When Rac1 was inhibited with EHT1864, decreased nuclear localization of YAP was found in vehicle, PXN overexpression and the mutant groups (Fig. 5B and D). Moreover, through sprouting angiogenesis assay, we found YAP inhibitor VP remarkably decreased sprout number and invasion distance in PXN overexpressing spheroids (Fig. 5E). Collectively, these data indicates that Rac1 activation is required for PXN phosphorylation-induced tip cell formation in stiffer matrix, and that YAP acts as the downstream mechanoeffector of PXN phosphorylation.

To further verify the role of p-PXN-Rac1-YAP activation in ECM stiffness-induced tip cell formation and angiogenesis in vivo, we created

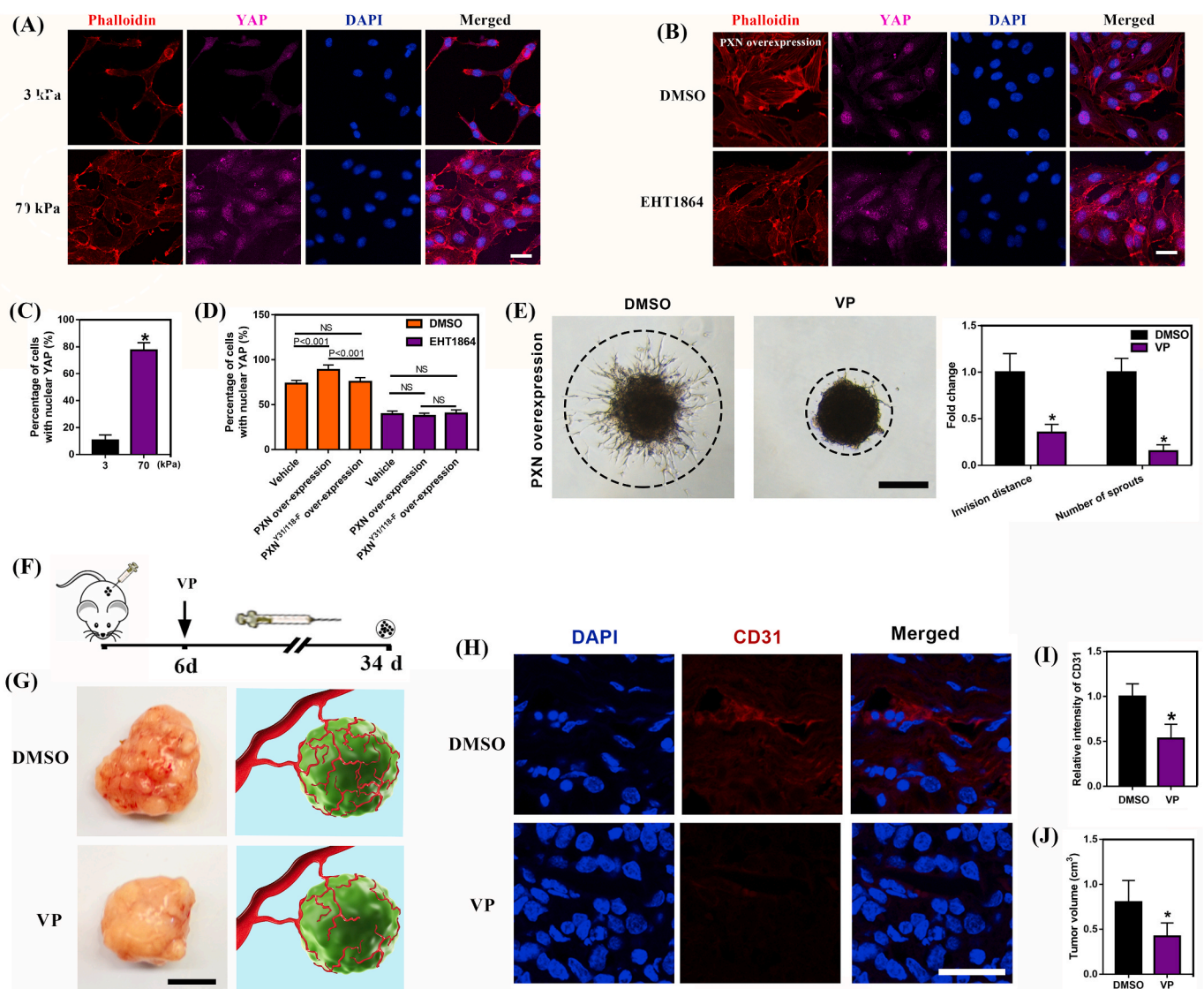


Fig. 5. p-PXN-Rac1 promotes tip cell formation and angiogenesis by activating YAP. (A) hUVECs on stiff ECM exhibited higher expression and increased nuclear localization of YAP. (Scale bar: 25 μm) (B) EHT1864 abrogated PXN overexpression induced increased YAP nuclear localization. (Scale bar: 25 μm) (C-D) Quantification analysis of YAP in (A, B), respectively. (E) Spheroid sprouting angiogenesis showed that VP inhibited sprouting angiogenesis of PXN overexpressing ECs. (Scale bar: 200 μm) (F) Schematic illustration of VP application in nude mice with xenograft. (G) Photographs of implants showed that sprouting angiogenesis was reduced by VP (Scale bar: 5 mm). (H-I) Angiogenesis and CD31 intensity of xenograft were significantly reduced by VP treatment (Scale bar: 25 μm). (J) VP decreased the volume of the xenograft. (*p < 0.05).

tumor models by subcutaneous injection of HepG2 cells in nude mice and treated with VP once a day from the 8th day (Fig. 5F). After 4 weeks, we found less sprouted blood vessels on tumor capsule (Fig. 5G) and decreased CD31, CD34 and VEGF intensity (Fig. 5H, I and Fig. S11) in VP treated group when compared to the control group, indicating that angiogenesis was obviously inhibited by VP. Moreover, VP treatment decreased tumor volume (Fig. 5J). Taken together, these data indicate p-PXN-Rac1-YAP signaling axis is heavily involved in tip cell formation and angiogenesis imposed by ECM stiffening.

Recent studies have found that YAP play key roles in the formation and morphogenesis of tip ECs. For example, Kim et al. [30] found that the tip ECs in *YAP/Taz^{ΔEC}* mice showed a blunted-end, aneurysm-like structure with fewer and dysmorphic filopodia compared with those of WT mice, while hyperactivation of YAP in mice resulted in excessive filopodia protrusions. Although the underlying mechanisms of how ECM stiffness regulates tip cell formation through YAP is unknown, deeper analysis of past studies sheds some light on this process. ECM stiffness activates YAP-dependent transcriptional program through mechanotransduction to regulate cytoskeletal rearrangement and metabolic activity during sprouting angiogenesis, which eventually contributes to morphogenesis and migration of tip cells [30,31,61]. Moreover, tip cell selection in vivo is highly dependent on cell rearrangement. Cruys et al. [62] have confirmed the link between EC rearrangements and metabolism by combining computational modelling with experimentation.

Therefore, alterations in metabolism of ECs caused by YAP activation through mechanotransduction could profoundly affect tip cell formation. However, further studies are needed to verify this hypothesis.

3.5. p-PXN loosens cell-cell connection facilitating matrix stiffness-regulated tip cell formation

In this research, we found that cells on compliant substrates formed continuous junctions between cells, whereas intercellular junctions on stiff substrates were punctate and discontinuous (Fig. 6A).

Similarly, Bordeleau et al. [55] has also reported that endothelial cadherin is altered as function of matrix stiffness, with minor proportions of VE-cadherin connected with cytoskeletal system of ECs on stiff matrix. We further observed that PXN overexpression increased the phosphorylation of VE-cadherin at Y-658 compared with the vehicle group, which was abolished by the mutant PXN (Fig. 3C). Since Y-658 phosphorylation prevents the binding of p120-to the cytoplasmic tail of VE-cadherin, phosphorylation at this site leads to the loosening of cell-cell contacts [63]. To further confirm that p-PXN-induced cell-cell connection loosening, we performed immunocytochemical staining for zona occludens 1 (ZO-1), a tight junction protein. The results showed that PXN overexpression not only decreased the intensity of ZO-1 staining, but also induced a punctate staining pattern at cell-cell junctions (Fig. 6B). Moreover, there was different subcellular distribution

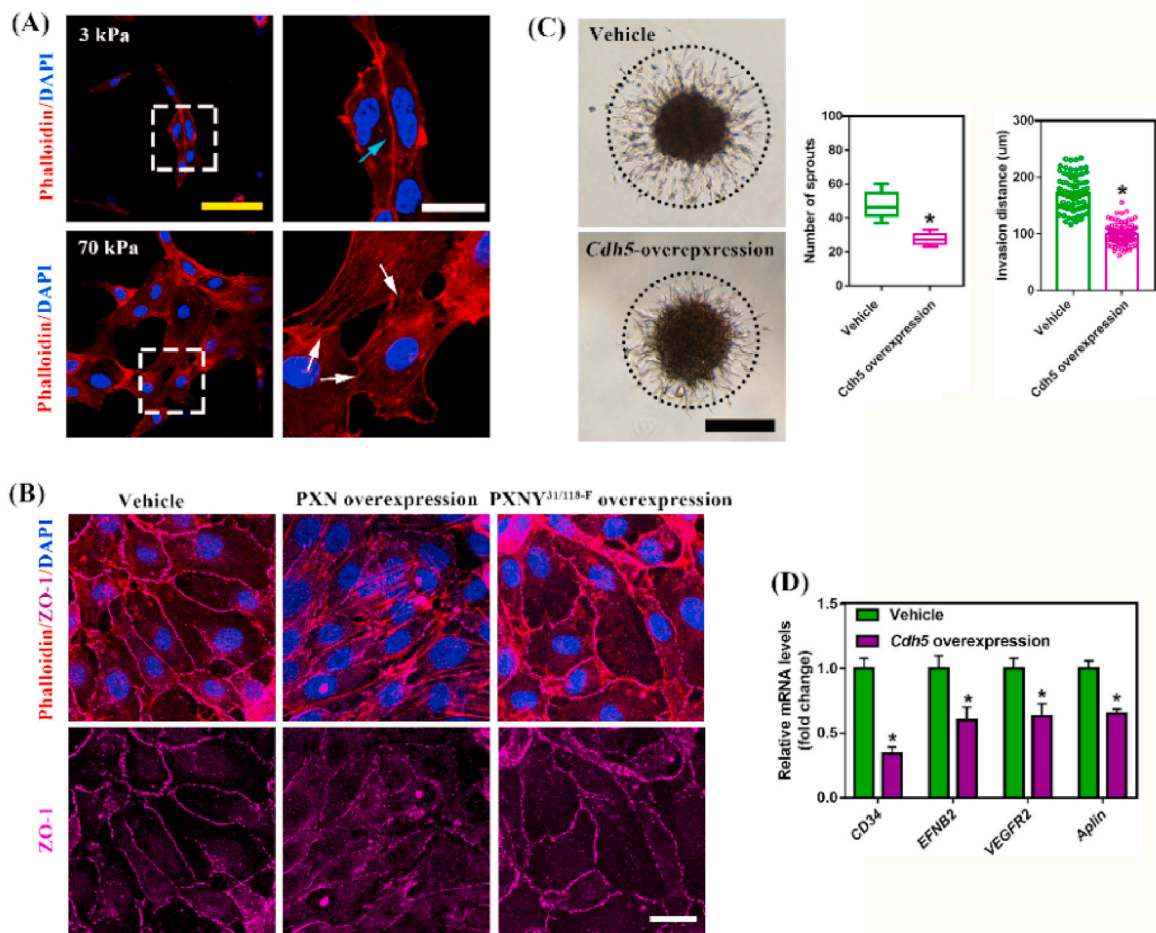


Fig. 6. p-PXN-induced decrease of intercellular connection is in part responsible for stiffening-mediated tip cell formation. (A) Cells on compliant substrates formed continuous junctions between cells, whereas the junctions on stiff substrates were punctate. (Marked by the white arrow, scale bars: left 75 μm, right 25 μm) (B) PXN overexpression not only decreased the intensity of ZO-1, but also induced a punctate pattern at cell-cell junctions (C) VE-cadherin overexpression decreased the outgrowth from the spheroids and resulted in fewer angiogenic sprouts (Scale bar: 200 μm). (D) mRNA levels of tip cell-enriched genes were decreased by VE-cadherin overexpression. (*p < 0.05).

among these groups, with more ZO-1 diffusing into the cytoplasm of PXN overexpressed cells, indicating partial destruction of the tight junction. Since tip cell formation might be associated with decreased intercellular junction [34,64], we then constructed a lentivirus to overexpress the *cdh5* gene in hUVECs (Fig. S12) to confirm the relationship between VE-cadherin and tip cell formation. We found that in sprouting assay of EC spheroids, overexpression of VE-cadherin decreased the outgrowth response from the spheroids (Fig. 6C) and decreased expression of tip cell-enriched genes (Fig. 6D), indicating that intercellular connection restricted tip cell formation. It could be deduced that p-PXN induced cell-cell connection loosening might be in part responsible for the stiffening-regulated tip cell formation.

Pathological angiogenesis and endothelial dysfunction are deeply implicated in the development of HCC. HCC often develops from advanced fibrosis and liver cirrhosis and is thus accompanied by increased stiffness. Mechanically, matrix stiffness upregulates VEGFR2 expression in ECs and VEGF expression in carcinoma cells through the integrin α V β 5/Akt/Sp1 signaling pathway and integrin β 1 activation, respectively [65,66]. Moreover, increasing matrix stiffness can also upregulate angiogenic angiopoietin-2 levels in ECs [67]. Due to the close relationship between matrix stiffness, angiogenesis and HCC development, the stiffness measurement of liver has become a strong predictor of HCC development and progression in the clinic. Nevertheless, the aforementioned mechanisms cannot explain the regulation of functional shift of quiescent ECs into tip cells by matrix stiffness, which is a key event during sprouting angiogenesis. Here, we propose that ECM mechanical properties contribute to tip cell formation through mechanotransduction by p-PXN-Rac1-YAP signaling axis (Fig. 7A–C). Once mechanical forces imposed by rigid ECM are detected at the cell surface of quiescent ECs, the information carried by focal adhesion complex including integrins, vinculin, FAK, Src and PXN must be propagated and transduced within the cytoskeleton. Specifically, phosphorylated PXN in FAs activates Rac1, which activate actin-regulatory proteins, such as actin-related protein 2/3 complex (ARP2/3) and Wiskott–Aldrich syndrome protein (WASP), to restructure the cytoskeleton [68]. Mechanotransduction leads to increased tension of actin cytoskeleton, reflected

by increased cellular stiffness on stiff ECM. Then, actin cytoskeleton with increased tension contributes to transfer of YAP from cytoplasm to nucleus and thus mechanosensing is ultimately linked to activity of nuclear transcription factors, thereby promotes tip cell specification. At the other hand, cell-cell connection is loosened by p-PXN which is also responsible for the stiffening-mediated tip cell formation.

Our study thus shed some light on the underlying mechanisms of matrix stiffness-regulated VE-Cadherin phosphorylation. Specifically, matrix stiffening promotes phosphorylation of PXN through mechanotransduction, thereby enhancing VE-Cadherin phosphorylation. Our results are consistent with a previous study showing that p-PXN induced phosphorylation of VE-Cadherin and its subsequent internalization and degradation [69]. However, how exactly the phosphorylation VE-Cadherin is induced by p-PXN is still unclear, which is a limitation of this study. To solve this problem, further investigations will be necessary.

4. Conclusion

In summary, our present research shed light on the role of mechanotransduction in tip cell specification and the underlying mechanism for the first time. This can not only deepen our understanding of the mechanism of tip cell formation and angiogenesis, but also help optimize the biomaterial design for tissue engineering and regenerative medicine and provide novel treatment strategies for some pathological situations. For either tissue engineering or the blood vessels regeneration, mechanical properties, such as stiffness aiming at tip cell formation should be taken into account to design optimal functional biomaterials. Moreover, ECM can stiffen under many pathological states, such as cancer progression. Since increased tip cell number increases surrounding stiffening cancer, it urgently calls for agents targeting p-PXN, Rac1 or YAP to effectively prevent growth and metastasis of tumor.

CRediT authorship contribution statement

Yaru Guo: Conceptualization, Methodology, Validation, Formal

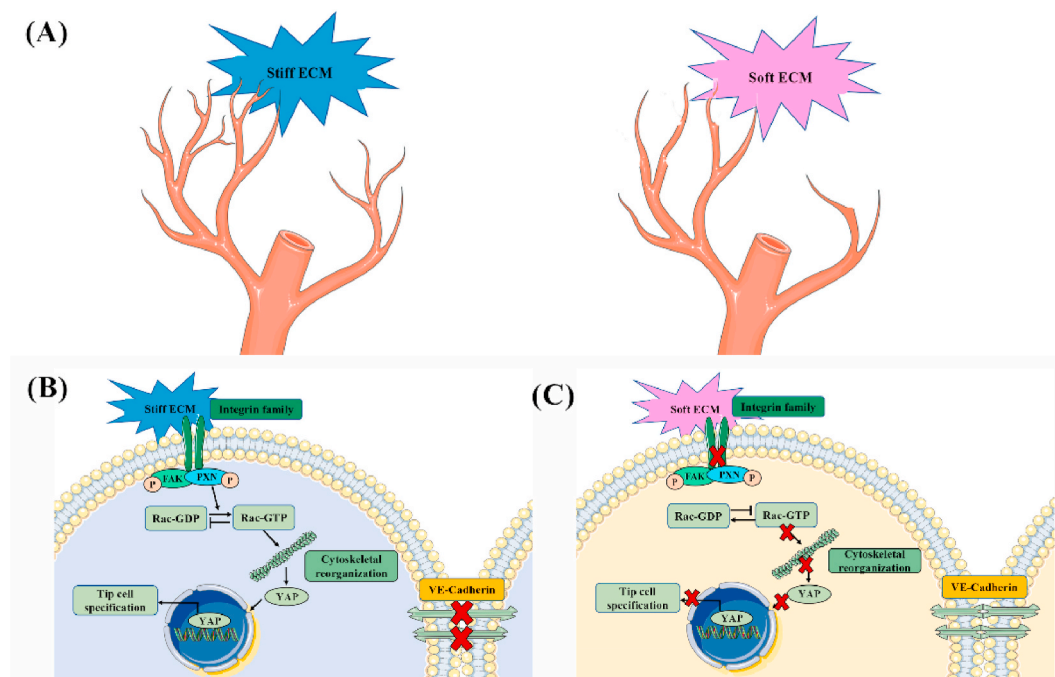


Fig. 7. Schematic diagram illustrating the underlying mechanisms, by which sprouting angiogenesis is affected by ECM stiffness. (A) Matrix stiffening promotes sprouting angiogenesis with more tip cells leading the vessel branches. (B) p-PXN-Rac1-YAP-induced mechanotransduction and decreased intercellular connection imposed by stiff matrix promote tip cell specification. (C) PXN-Rac1-YAP signaling is inhibited and intercellular connection is increased by soft ECM, which inhibits tip cell formation.

analysis, Investigation, Data curation, Writing – original draft, Visualization. **Feng Mei**: Investigation, Data curation, Writing – original draft. **Ying Huang**: Methodology, Data curation, Software. **Siqin Ma**: Methodology, Data curation, Software. **Yan Wei**: Investigation, Data curation, Writing – review & editing. **Xuehui Zhang**: Resources, Funding acquisition, Writing – review & editing. **Mingming Xu**: Software, Investigation. **Ying He**: Software, Investigation. **Boon Chin Heng**: Funding acquisition, Writing – review & editing. **Lili Chen**: Conceptualization, Supervision, Writing – review & editing. **Xuliang Deng**: Conceptualization, Writing – review & editing, Supervision, Funding acquisition, Project administration.

Declaration of competing interest

The authors declare that they have no known competing financial interests or personal relationships that could have appeared to influence the work reported in this paper.

Acknowledgements

This work was supported by the National Key R&D Program of China (2018YFC1105303/04), National Natural Science Foundation of China (Nos. 81991505, 82022016, 51772006, 31670993, 51973004) and Beijing Municipal Science & Technology Commission Projects (Z181100002018001). We thank Dr. Siying Qin at the National Center for Protein Sciences of Peking University for technical help with AFM.

Appendix A. Supplementary data

Supplementary data to this article can be found online at <https://doi.org/10.1016/j.bioactmat.2021.05.033>.

References

- [1] S. Huang, D. Lei, Q. Yang, et al., A perfusable, multifunctional epicardial device improves cardiac function and tissue repair, *Nat. Med.* 27 (2021) 480–490.
- [2] H. Park, H. Yamamoto, L. Mohn, et al., Integrin-linked kinase controls retinal angiogenesis and is linked to Wnt signaling and exudative vitreoretinopathy, *Nat. Commun.* 10 (2019) 5243.
- [3] Y.H. Kim, J. Choi, M.J. Yang, et al., A MST1–FOXO1 cascade establishes endothelial tip cell polarity and facilitates sprouting angiogenesis, *Nat. Commun.* 10 (2019) 838.
- [4] W. Chen, P. Xia, H. Wang, et al., The endothelial tip-stalk cell selection and shuffling during angiogenesis, *J. Cell Commun. Signal.* 13 (2019) 291–301.
- [5] D.J. Page, R. Thuret, L. Venkatraman, et al., Positive feedback defines the timing, magnitude, and robustness of angiogenesis, *Cell Rep.* 27 (2019) 3139–3151.
- [6] A.F. Siekmann, N.D. Lawson, Notch signalling limits angiogenic cell behaviour in developing zebrafish arteries, *Nature* 445 (2019) 781–784.
- [7] Wei Yanhong, Junsong Gong, K. Thimmulappa Rajesh, et al., Nrf2 acts cell-autonomously in endothelium to regulate tip cell formation and vascular branching, *Proc. Natl. Acad. Sci. U. S. A.* 110 (2013) E3910–E3918.
- [8] Yannick Blum, Belting Heinz-Grogr, Ellertsdottir Elin, et al., Complex cell rearrangements during intersegmental vessel sprouting and vessel fusion in the zebrafish embryo, *Biophys. J.* 316 (2008) 312–322.
- [9] C.H. Kuo, Y.H. Huang, P.K. Chen, et al., VEGF-induced endothelial podosomes via ROCK2-dependent thrombomodulin expression initiate sprouting angiogenesis, *Arterioscler. Thromb. Vasc. Biol.* 41 (2021) 1657–1671.
- [10] G. Dallinga Marchien, I. Habani Yasmin, W.M. Schimmel Alinda, et al., The role of heparan sulfate and neuropilin 2 in VEGFA signaling in human endothelial tip cells and non-tip cells during angiogenesis in vitro, *Cells* 10 (2021) 926.
- [11] Qiu Jiang, Mariana Lagos-Quintana, Dong Liu, et al., miR-30a regulates endothelial tip cell formation and arteriolar branching, *Hypertension* 62 (2013) 592–598.
- [12] Larrivé Bruno, Prahst Claudia, Emma Gordon, et al., ALK1 signaling inhibits angiogenesis by cooperating with the Notch pathway, *Dev. Cell* 22 (2012) 489–500.
- [13] Goveia Jermaine, Zecchin Annalisa, Francisco Morales Rodriguez, et al., Endothelial cell differentiation by SOX17: promoting the tip cell or stalking its neighbor instead? *Circ. Res.* 115 (2014) 205–207.
- [14] E. Discher Dennis, Janmey Paul, Yu-li Wang, Tissue cells feel and respond to the stiffness of their substrate, *Science* 310 (2005) 1139–1143.
- [15] Chenghu Zhang, Ting Zhou, Zhipeng Chen, et al., Coupling of integrin $\alpha 5$ to annexin A2 by flow drives endothelial activation, *Circ. Res.* (2020) 127.
- [16] Givens Chris, Tzima Ellie, Endothelial mechanosignaling: does one sensor fit all? *Antioxidants Redox Signal.* 25 (2016) 373–388.
- [17] B. Jung, H. Obinata, S. Galvani, et al., Flow-regulated endothelial S1P receptor-1 signaling sustains vascular development, *Dev. Cell* 23 (2012) 600–610.
- [18] O.O. Arishe, A.B. Ebeigbe, W.R. Clinton, Mechanotransduction and uterine blood flow in preeclampsia: the role of mechanosensing piezo 1 ion channels, *Am. J. Hypertens.* (2019) 1.
- [19] Y.J. Chiu, E. Mcbeath, K. Fujiwara, Mechanotransduction in an extracted cell model: fyn drives stretch- and flow-elicited PECAM-1 phosphorylation, *J. Cell Biol.* 182 (2008) 753–763.
- [20] B.G. Coon, N. Baeyens, J. Han, et al., Intramembrane binding of VE-cadherin to VEGFR2 and VEGFR3 assembles the endothelial mechanosensory complex, *J. Cell Biol.* 208 (2015) 975–986.
- [21] Jalali Shila, A. del Pozo Miguel, Kuang Den Chen, et al., Integrin-mediated mechanotransduction requires its dynamic interaction with specific extracellular matrix (ECM) ligands, *Proc. Natl. Acad. Sci. Unit. States Am.* 98 (2001) 1042–1046.
- [22] Zebda Noureddine, Dubrovskiy Oleksii, G. Birukov Konstantin, Focal adhesion kinase regulation of mechanotransduction and its impact on endothelial cell functions, *Microvasc. Res.* 83 (2012) 71–81.
- [23] Shira Landau, Ben-Shaul Shahar, Levenberg Shulamit, Oscillatory strain promotes vessel stabilization and alignment through fibroblast YAP-mediated mechanosensitivity, *Adv. Sci.* 5 (2018), 1800506.
- [24] D. Ross Tyler, G. Coon Brian, Sanguk Yun, et al., Integrins in mechanotransduction, *Curr. Opin. Cell Biol.* 25 (2013) 613–618.
- [25] P. Maruri Daniel, Miron-Mendoza Miguel, B. Kivanany Pouriska, et al., ECM stiffness controls the activation and contractility of corneal keratocytes in response to TGF- β 1, *Biophys. J.* 119 (2020) 1865–1877.
- [26] A.D. Vita, C. Liverani, R. Molinaro, et al., Lysyl oxidase engineered lipid nanovesicles for the treatment of triple negative breast cancer, *Sci. Rep.* 11 (2021) 5107.
- [27] Bordeleau Francois, N. Masona Brooke, Macklin Lollisb Emmanuel, et al., Matrix stiffening promotes a tumor vasculature phenotype, *Proc. Natl. Acad. Sci. U. S. A.* 114 (2017) 492–497.
- [28] Sirio Dupont, Morsut Leonardo, Aragona Mariaceleste, et al., Role of YAP/TAZ in mechanotransduction, *Nature* 474 (2011) 179–183.
- [29] N. Filipa, K.B. Alexandra, O.Y. Ting, et al., YAP and TAZ regulate adherens junction dynamics and endothelial cell distribution during vascular development, *eLife* 7 (2018), e31037.
- [30] Jongshin Kim, Hyung Kim Yoo, Jaeryung Kim, et al., YAP/TAZ regulates sprouting angiogenesis and vascular barrier maturation, *J. Clin. Invest.* 127 (2017) 3441–3461.
- [31] Xiaohong Wang, Valls Aida Freire, Schermann Géza, et al., YAP/TAZ orchestrate VEGF signaling during developmental angiogenesis, *Dev. Cell* 42 (2017) 462–478.
- [32] Cen Cao, Ying Huang, Qingming Tang, et al., Bidirectional juxtacrine ephrinB2/Ephs signaling promotes angiogenesis of ECs and maintains self-renewal of MSCs, *Biomaterials* 172 (2018) 1–13.
- [33] M. Fischer, D. Wessler, K.J. Henrichs, et al., Influence of beta-aminopropionitril on media hypertrophy and baroreceptor reflex in normotensive and hypertensive rats, *J. Hypertens. Suppl. Off. J. Int. Soc. Hypertens.* 4 (1986) S527.
- [34] Jiahui Cao, Ehling Manuel, Marz Sigrid, et al., Polarized actin and VE-cadherin dynamics regulate junctional remodelling and cell migration during sprouting angiogenesis, *Nat. Commun.* 8 (2017) 2210.
- [35] A.E. German, Paxillin-dependent Control of Tumor Angiogenesis, vol. 1, Massachusetts Institute of Technology, 2014, pp. 1–136.
- [36] S. Ogawa, F. Moriyasu, K. Yoshida, et al., Relationship between liver tissue stiffness and histopathological findings analyzed by shear wave elastography and compression testing in rats with non-alcoholic steatohepatitis, *J. Med. Ultrason.* 43 (2016) 355–360.
- [37] Sztilkovics Milan, Gerecsei Tamas, Beatrix Peter, et al., Single-cell adhesion force kinetics of cell populations from combined label-free optical biosensor and robotic fluidic force microscopy, *Sci. Rep.* 10 (2020), 61.
- [38] S.G. Szeto, M. Narimatsu, M. Lu, et al., YAP/TAZ are mechanoregulators of TGF- β -smad signaling and renal fibrogenesis, *J. Am. Soc. Nephrol.* 27 (2016) 3117–3128.
- [39] Guilai Liu, Honisch Sabina, Guoxing Liu, et al., Up-regulation of Orai 1 expression and store operated Ca(2+) entry following activation of membrane androgen receptors in MCF-7 breast tumor cells, *BMC Cell.* (2015) 1–10.
- [40] L. Désiré, J. Bourdin, N. Loiseau, et al., RAC1 inhibition targets amyloid precursor protein processing by γ -secretase and decreases $a\beta$ production in vitro and in vivo *, *J. Biol. Chem.* 280 (2005) 37516–37525.
- [41] Stutchbury Ben, Atherton Paul, Ricky Tsang, et al., Distinct focal adhesion protein modules control different aspects of mechanotransduction, *J. Cell Sci.* 130 (2017) 1612–1624.
- [42] E. Donohue, A. Thomas, N. Maurer, et al., The autophagy inhibitor verteporfin moderately enhances the antitumor activity of gemcitabine in a pancreatic ductal adenocarcinoma model, *J. Canc.* 4 (2013) 585–596.
- [43] I. Lopez Jose, Inkyung Kang, Weon Kyoo You, et al., In situ force mapping of mammary gland transformation, *Integr. Biol. Quantitat. Biosci. Nano Macro* 3 (2011) 910.
- [44] R. Levental Kandice, Hongmei Yu, Kass Laura, et al., Matrix crosslinking forces tumor progression by enhancing integrin signaling, *Cell* 139 (2009) 891–906.
- [45] Chen Ying Chieh, Rwei Zeng Lin, Hao Qi, et al., Functional human vascular network generated in photocrosslinkable gelatin methacrylate hydrogels, *Adv. Funct. Mater.* 22 (2012) 2027–2039.
- [46] R. Pfeifer Charlotte, M. Alvey Cory, Irianto Jerome, et al., Genome variation across cancers scales with tissue stiffness - an invasion-mutation mechanism and implications for immune cell infiltration, *Curr. Opin. Struct. Biol.* 2 (2017) 103–114.
- [47] Andreas Benn, Hiepen Christian, Osterland Marc, et al., Role of bone morphogenetic proteins in sprouting angiogenesis: differential BMP receptor-

- dependent signaling pathways balance stalk vs. tip cell competence, *Faseb. J.* 31 (2017) 4720–4733.
- [48] J. Siemerink Martin, Ingeborg Klaassen, M.C. Vogels Ilse, et al., CD34 marks angiogenic tip cells in human vascular endothelial cell cultures, *Angiogenesis* 15 (2012) 151–163.
- [49] A. Strasser Geraldine, S. Kaminker Joshua, Marc Tessier Lavigne, Microarray analysis of retinal endothelial tip cells identifies CXCR4 as a mediator of tip cell morphology and branching, *Blood* 115 (2010) 5102–5110.
- [50] G. Dallinga Marchien, , Yetkin-Arik Bahar, P. Kayser Richelle, et al., IGF2 and IGF1R identified as novel tip cell genes in primary microvascular endothelial cell monolayers, *Angiogenesis* 21 (2018) 823–836.
- [51] T. Edgar Lowell, J. Underwood Clayton, E. Guilkey James, et al., Extracellular matrix density regulates the rate of neovessel growth and branching in sprouting angiogenesis, *PLoS One* 9 (2014), e85178.
- [52] M. Ghajar Cyrus, Xiaofang Chen, W. Harris Joseph, et al., The effect of matrix density on the regulation of 3-D capillary morphogenesis, *Biophys. J.* 94 (2008) 1930–1941.
- [53] Zioli Marianne, Handra-Luca Adriana, Kettaneh Adrien, et al., Noninvasive assessment of liver fibrosis by measurement of stiffness in patients with chronic hepatitis C, *Hepatology* 41 (2005) 48–54.
- [54] L. Castera, X. Forns, A. Alberti, Non-invasive evaluation of liver fibrosis using transient elastography, *J. Hepatol.* 48 (2008) 835–847.
- [55] F. Bordeleau, B.N. Mason, E.M. Lollis, et al., Matrix stiffening promotes a tumor vasculature phenotype, *Proc. Natl. Acad. Sci. U. S. A.* 114 (2017) 492–497.
- [56] Halder Georg, Sirio Dupont, Piccolo Stefano, Transduction of mechanical and cytoskeletal cues by YAP and TAZ, *Nat. Rev. Mol. Cell Biol.* 13 (2012) 591–600.
- [57] O.Y. Revach, I. Grosheva, B. Geiger, Biomechanical regulation of focal adhesion and invadopodia formation, *J. Cell Sci.* 133 (2020), jcs244848.
- [58] J. Paszek Matthew, Zahir Nastaran, R. Johnson Kandice, et al., Tensional homeostasis and the malignant phenotype, *Canc. Cell* 8 (2005) 241–254.
- [59] Yuki Toyama, Kontani Kenji, Katada Toshiaki, et al., Decreased conformational stability in the oncogenic N92I mutant of Ras-related C3 botulinum toxin substrate 1, *Sci. Adv.* 5 (2019) 1595.
- [60] C. Onesto, A. Shutes, V. Picard, et al., Characterization of EHT 1864, a novel small molecule inhibitor of rac family small GTPases, *Methods Enzymol.* 439 (2008) 111–129.
- [61] Bertero Thomas, M. Oldham William, A. Cottrill Katherine, et al., Vascular stiffness mechanoactivates YAP/TAZ-dependent glutaminolysis to drive pulmonary hypertension, *J. Clin. Invest.* (2016) 126.
- [62] Cruys Bert, W. Wong Brian, Kuchnio Anna, et al., Glycolytic regulation of cell rearrangement in angiogenesis, *Nat. Commun.* 7 (2016), 12240.
- [63] Panfeng Fu, Ramchandran Ramaswamy, Shaaya Mark, et al., Phospholipase D2 restores endothelial barrier function by promoting PTPN14-mediated VE-cadherin dephosphorylation, *J. Biol. Chem.* 295 (2020) 7669–7685.
- [64] Sabu Abraham, Yeo Margaret, Montero-Balaguer Mercedes, et al., VE-Cadherin-mediated cell-cell interaction suppresses sprouting via signaling to MLC2 phosphorylation, *Curr. Biol.* 19 (2009) 668–674.
- [65] Chenghu Zhang, Ting Zhou, Zhipeng Chen, et al., Coupling of integrin $\alpha 5$ to annexin A2 by flow drives endothelial activation, *Circ. Res.* 127 (2020) 1074–1090.
- [66] F. Broders-Bondon, Ho-Bouloires Thn, M.E. Fernandez-Sanchez, et al., Mechanotransduction in tumor progression: the dark side of the force, *JCB (J. Cell Biol.)* 217 (2018) 1571–1587.
- [67] Yosuke Osawa, Yoshio Sachiyo, Yoshihiko Aoki, et al., Blood angiopoietin-2 predicts liver angiogenesis and fibrosis in hepatitis C patients, *BMC Gastroenterol.* 21 (2021) 55.
- [68] W. Sun, J. Yang, Y. Hong, et al., Lanthanum chloride impairs learning and memory and induces dendritic spine abnormality by down-regulating Rac1/PAK signaling pathway in Hippocampus of offspring rats, *Cell. Mol. Neurobiol.* 40 (2019) 459–475.
- [69] Dragoni Silvia, Natalie Hudson, Bridget Ann Kenny, et al., Endothelial MAPKs direct ICAM-1 signaling to divergent inflammatory functions, *J. Immunol.* (2017) 4074–4085.